STUDY OF PLASMONIC SILVER NANOPARTICLES SYNTHESIZED BY CONVENTIONAL AND ECO-FRIENDLY METHODS WITH ULTRAVIOLET IRRADIATION

R. PLESNICUTE[1], M. ELUTA[1], A. LES-AGAVRILOAEI[1], I. MOTRESCU[2], L. OPRICA[3], D. CREANGA[1,*]

[1]Alexandu Ioan Cuza University, Physics Faculty, Iasi, Romania
E-mail: dorina.emilia.creanga@gmail.com
[2] Ion Ionescu de la Brad University of Life Sciences, Iasi, Romania
[3]Alexandu Ioan Cuza University, Biology Faculty, Iasi, Romania
[*] *Corresponding author, E-mail*: dorina.emilia.creanga@gmail.com

Received July 6, 2024

Abstract. The synthesis of some silver nanoparticles was carried out by two-step reduction, with chemical or biological antioxidants, and subsequent exposure to ultraviolet radiation. Synthesis efficiency was progressively increased after 30 min during second step: about 40% increase of LSPR band intensity for chemical reducing and more than 100% enhancing for biological reducing.

Key words: Silver reducing, electro-optical features, eco-friendly approach.

DOI: https://doi.org/10.59277/RomJPhys.2024.69.618

1. INTRODUCTION

The wide spread of silver nanoparticle (AgNP) uses in people daily life raised the concern of their fate in the environment, thus various studies are developed to control not only the nanoparticle properties and applications but also their ecological impact.

The huge quantities of silver particles that are produced every year – according to statistics [1], exploit both the antiseptic properties – in the chemical and pharmaceutical as well as the textile industry, and the special optical and spectral characteristics that recommends silver nanoparticles primarily for optoelectronics, markers, and sensoristic.

Like other noble metals, especially gold, silver nanoparticles exhibit the phenomenon of Localized Surface Plasmon Resonance (LSPR). This phenomenon [2, 3] is the result of the surface metal atom response to the incident light radiation [4, 5] that induces at the electron level a collective oscillation, *i.e.* the generation of a field electromagnetic located on particle surface.

Due to the plasmonic emission in the visible range – that covers a volume of two order of magnitude larger than the source particle, AgNP visualization in Dark Field Optical Microscopy is possible, which doesn't happen for magnetic nanoparticles, for instance.

Regarding the synthesis efficacy by chemical reduction with citrate – quite productive for gold nanoparticles, the main options are either the addition of supplementary reagents such as sodium borohydrate [6] or tannic acid [7, 8] or performing the reaction under the simultaneous impact of UV radiation [9, 10]. For increased biocompatibility and suitable environmental protection, it is the biological synthesis that was diversified by using plant extracts, for example. Juice extracted from orange [11], papaya [12] and apple [13] or zest extract of lemon [14, 15] or ananas [16] were successfully tested as antioxidant sources able to reduce silver ions from silver nitrate.

We report some results regarding a proposed two-step procedure, that combines silver reducing with chemical or biological antioxidants with subsequent exposure to ultraviolet radiation and could be applied to both chemical conventional synthesis with citrate and eco-friendly synthesis with lemon fruit extract.

2. EXPERIMENTAL

2.1. NANOPARTICLE SYNTHESIS

Method 1. Silver chemical reducing was performed by applying basically Turkevich method [17] with trisodium citrate dihydrate (TSC, $C_6H_9Na_3O_9$), 50 mL 1% (w/v) against 50 mL of 1 mM $AgNO_3$ solution. The reagents were let to heat at about 80°C, under continuous magnetic stirring at 800 rpm until the color of the mixture turned off to pale yellow.

The UV-C exposure was carried out for no more than 30 min (10-20-30 min with 10 min breaks) aiming the adjusting of process duration and costs.

The reaction mechanism of chemical reduction of silver ions (Ag^+) from silver nitrate ($AgNO_3$), dissociated in water as silver atoms (Ag^0), can be written as [18]:

$$4Ag^+ + C_6H_5O_7Na_3 + 2H_2O \rightarrow 4Ag^0 + C_6H_5O_7H_3 + 3Na^+ + H^+ + O_2\uparrow \quad (1)$$

Method 2. Silver biological reducing was accomplished with fresh lemon fruit extract (rich in citric and tannic acids as well as in larger antioxidant molecules like flavonoids, carotenoids, pectins, etc.), from commercially available *Citrus lemon* fruits.

The fruit extract was centrifuged at 5000 rpm for 15 minutes to get the supernatant for the silver reduction (12.5 mL volume of the supernatant against 50 mL of 1 mM $AgNO_3$ like previously). The reaction vessel was let to heat at about 80°C under magnetic stirring (800 rpm) until the color turned off from pale yellow to brownish [19].

According to [20] the silver reduction with lemon fruit antioxidants can be written as follows:

$$4Ag^{+} + C_6H_5O_7 + X + 2H_2O \rightarrow 4Ag^{0} + C_6H_5O_7H_3 + H^{+} + Y + O_2\uparrow \quad (2)$$

where $C_6H_5O_7$ is the citric acid while X is another (main) antioxidant from lemon juice which helped in reduction of silver ions and transforms into its oxidized form, Y.

UV-C irradiation. The UV lamp (from Philips) was a low-pressure mercury vapor discharge tube that emits UV-C radiation with a peak at 253.7 nm (mercury line). The total UV power was 30 W while the UV-C radiation power was 12 W, according to producer specifications. Tube length was L = 0.87 m while D = 0.25 m was the distance from the horizontal tube to the beneath placed sample. The exposure was carried out on 10 mL of AgNP suspension in a 3 cm diameter uncovered vessel. UV-C energy, E ($E = I \times S \times t$), was ranging between 3.5 and 11.5 J for 10 to 30 min exposure (with 10 min breaks), the irradiance, I (Wm^{-2}), being given by Keitz formula (Eq. 3):

$$P = \frac{2\pi DLI}{(2\alpha + \sin 2\alpha)} \quad (3)$$

according to [21], while S was the vessel surface and t is the irradiation duration.

2.2. NANOPARTICLE INVESTIGATION METHODS

Shimadzu Lab 6000 X-ray diffractometer with Cu-Kα radiation having λ = 1.5406 Å, (20°–80° of 2θ range, scanning angle step of 0.02° and 0.5°/min scan speed) was used for crystallinity features identification.

Scanning Electron Microscopy (SEM) and Energy Dispersive X-Ray Spectroscopy (EDS) analyses were applied with ESEM device type Quanta 450 (FEI-ThermoScientific, USA) with EDAX module\(type Ametek Inc., USA) mounted inside the ESEM device chamber.

Shimadzu PharmaSpec 1600 device, with 1 cm quartz cells and specialized software for the acquisition and processing of spectral data was utilized for the LSPR (Localized Surface Plasmon Resonance) spectral band recording, analysis and graphical representation. Distilled water was the spectral reading blind sample.

An Optical Microscope with Dark Field module and 40 × objective, with video camera and dedicated software, was used for image capturing of nanoparticle plasmonic emission. ImageJ software was used for particle size analysis. Origin software package was useful in the statistical analysis of measured diameters with size histogram representation and lognormal function.

3. RESULTS AND DISCUSSION

3.1. SEM INVESTIGATION RESULTS

In Fig. 1a, for AgNP-TSC sample, the smallest nanoparticles evidenced in the SEM image appear to have mostly 20 nm size and symmetrical shape while largest particles and particle aggregates were found to have sizes over one hundred nm (in yellow squares), as in Fig. 2a. In Fig. 1b, for AgNP-lemon sample, one can see a more complex image, with many nanostructures either individual or as short clusters, up to 50 nm size according to Fig. 2b, their mineral and organic coating (vitamins, flavonoids, carotenoids, pectins etc.) influencing the contour delimitation and even suggesting certain organic nanostructures.

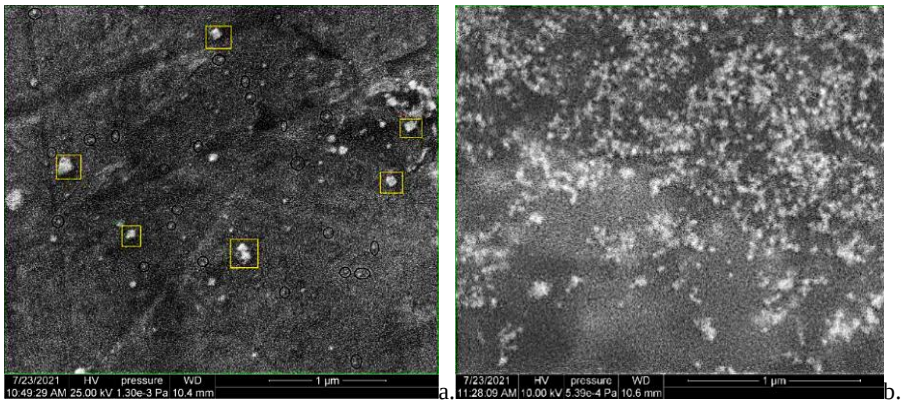

a. b.

Fig. 1 – SEM images: a) AgNPs synthesized by TSC chemical reduction; b) AgNPs synthesized with lemon fruit extract.

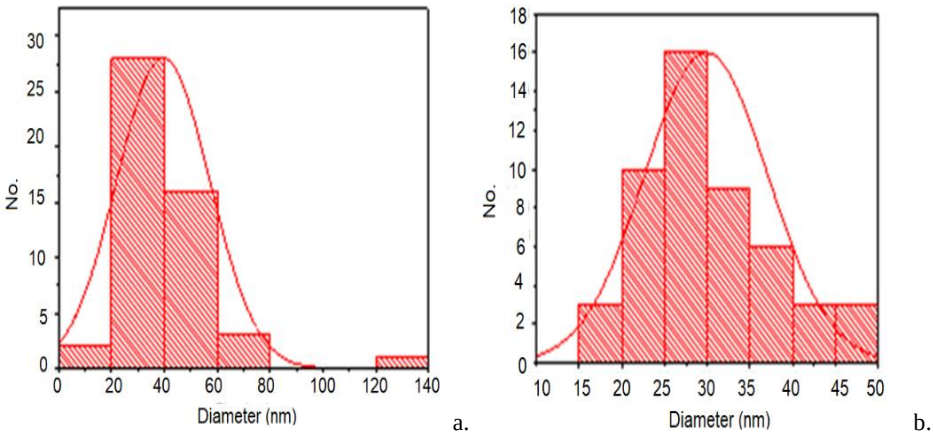

a. b.

Fig. 2 – Diameter histograms: a) AgNP-TSC; b) AgNP-lemon.

The nanoparticle diameter histograms (Fig. 2a, b) were fitted with log-normal function that evidenced, for AgNP-TSC, the mean value of 29.8 nm, with 7.2 nm standard deviation and, for AgNP-lemon, a larger mean value of 39.5 nm, with 7.6 nm standard deviation.

3.2. EDS ANALYSIS RESULTS

In AgNP-TSC sample (Fig. 3a) silver emission line (AgL) was emphasized as corresponding to 5.05% from the sample elements weights at the representative analyzed spot and 1.33% from elements abundance.

The highest peak corresponds to the aluminum support while copper is present as an impurity from the device inside room. According to Fig. 3b, in AgNP-lemon sample, the silver is present as 1.25% of the sample element weights at the analyzed spot and 0.18% from elements abundance, the carbon and oxygen originating from the organic components (mainly citrate ions attached to AgNP surface and acting as stabilizing capping (coating) agent).

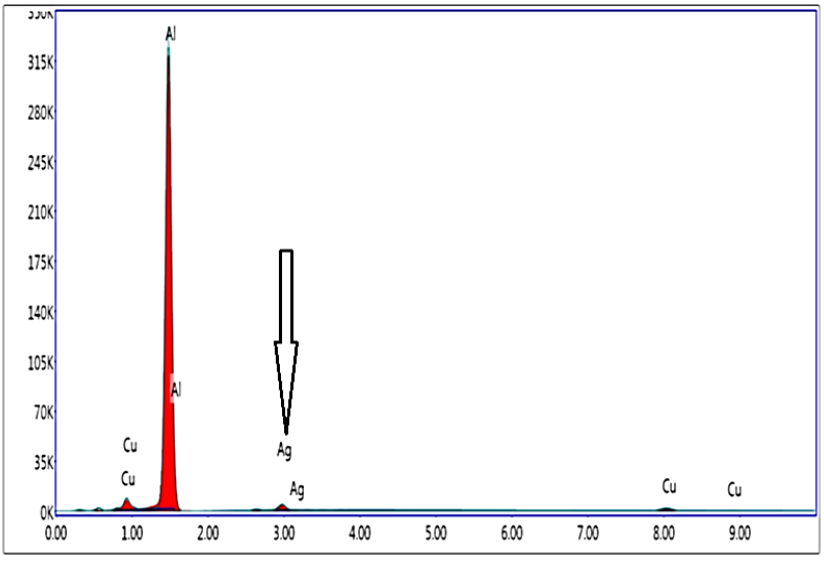

Element	Weight %	Atomic %	Net Int.	Error %
AlK	92.69	97.66	111,378.10	3.45
AgL	5.05	1.33	1,762.14	4.68
CuK	2.26	1.01	1,069.87	2.93

Fig. 3a – EDS analysis result for AgNP-TSC.

Copper is also present as an impurity in the installation or in the sample metal support.

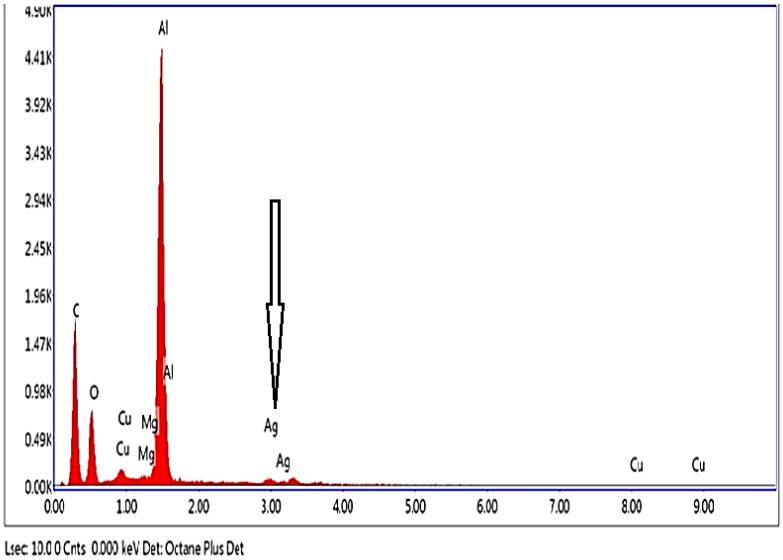

Element	Weight %	Atomic %	Net Int.	Error %
C K	51.71	66.21	1,352.05	10.47
O K	18.54	17.82	633.97	11.67
CuL	1.40	0.34	72.17	14.74
MgK	0.19	0.12	31.14	33.96
AlK	26.91	15.33	4,514.27	4.13
AgL	1.25	0.18	54.02	20.98

Fig. 3b – EDS analysis result for AgNP-lemon.

It could be hypothesized that the coating shell of AgNP-lemon structures, with many molecular components with high molecular weight and large sizes makes that EDS analyzed spots contain lower amount of silver than in the case of citrate thin coating layer for AgNP-TSC.

3.3. CRYSTALLINITY PROPERTIES

Silver XRD peaks were identified as (111), (200), (220), (311), according to JCPDS no. 19-0629 standard, denoting cubical crystallization of AgNPs. Recording noise was more significant for AgNP-lemon structures while amorphous phase was evidenced at small angles' domain, under 40 degrees (representing the glass support) in both samples. Unpredicted crystalline structures at 2θ angle of about 32–33

degrees, denoted with (*), might represent the reducer molecules acting also as stabilizer coatings [22].

Or there could be some AgO traces that generated the diffraction maxima denoted with (*) and also with arrow in Fig. 4a, b, according to [23]. Indeed, it is possible that certain oxidization of silver at the nanoparticle surface happens in the complex reaction medium. To calculate the crystallite average size, Scherrer formula was applied (Eq. 4):

$$D_{hkl} = \frac{K \cdot \lambda}{\beta \cdot \cos \theta_{hkl}} \quad (4)$$

where D_{hkl} is the crystallite size corresponding to the diffraction peak with (*hkl*) Miller' indexes and having θ_{hkl} as position on the horizontal axis (the Bragg angle), *K* is the shape factor (close to unity, taken as 0.9), λ is the diffractometer X-ray wavelength, and β is the line broadening at half the maximum intensity.

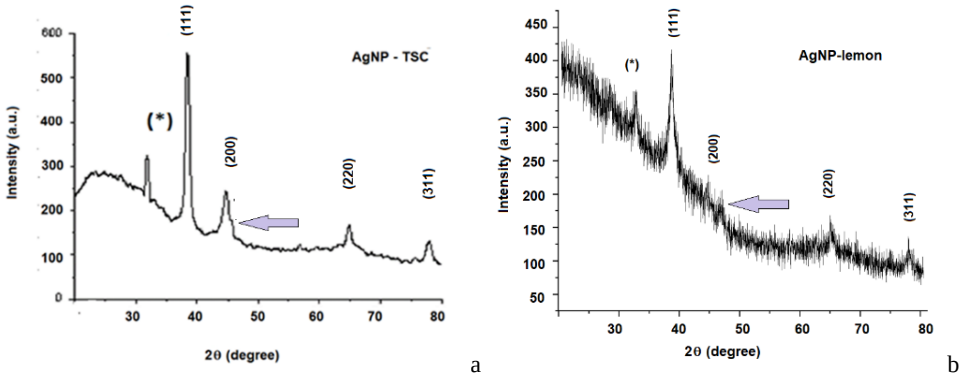

a b

Fig. 4 – XRD diagram for: a) AgNP-TSC sample; b) AgNP-lemon sample.

The values we have obtained for (111) peak are not much different, being of about 11 nm and 10.5 nm respectively, for AgNP-TSC and, respectively, AgNP-lemon sample. The lattice parameter, *a*, was also estimated with Eq. 5:

$$\frac{1}{d_{hkl}^2} = \frac{h^2+k^2+l^2}{a^2} \quad (5)$$

as function on the interplanar distance d_{hkl} (Eq. 6):

$$d_{hkl} = \frac{\lambda}{2 \cdot \sin \theta_{hkl}} \quad (6)$$

The lattice parameter was found to be 0.41 nm in both cases, in concordance with [24].

3.4. PLASMONIC PROPERTIES OF AGNPS

3.4.1. AgNPs reduced with TSC

Citrate acts as a relatively modest reducer for silver ions [25] but it is good stabilizer in colloidal suspension.

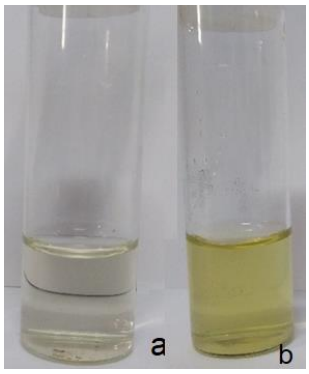

Fig. 5 – UV-C influence on silver reduction, using trisodium citrate:
a) sample before UV exposure; b) sample exposed 30 min to UV radiation.

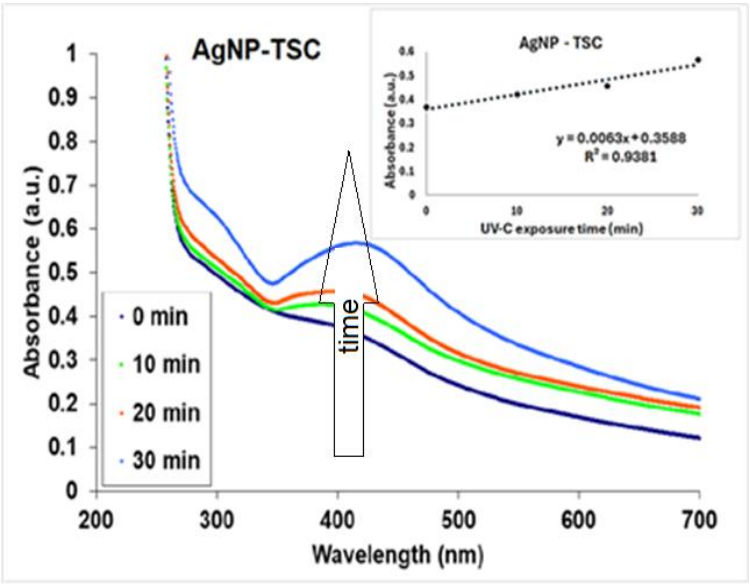

Fig. 6 – The influence of UV-C radiation on the LSPR band of AgNP-TSC. Image inset-the spectral band intensity increased linearly with UV-C exposure time.

The reduction reaction could be completed with UV-C energy absorption, which induced water photolysis. Hydroxyl ions released through water photolysis

can reduce supplementary silver ions in the reaction medium to form other AgNPs that intensified the suspension color, from pale yellow to intense yellow (Fig. 5) and increased the intensity of the characteristic band (Fig. 6).

Before the UV-C exposure, the characteristic spectral band is broad denoting polydispersity and had the maximum intensity of about 0.37 a.u. intensity (at 421 nm). As known, compared to uncoated silver nanoparticles that exhibit LPSR band at 400 nm or less, the nanoparticles stabilized by molecular shell have the characteristic band maximum shifted to the red domain of visible spectrum [26].

The UV-C exposure increased the reduction efficacy: maximum intensity reached 0.57 a.u. (at 418 nm) after 30 min (Fig. 6) *i.e.* 50% increase. Slight blue shift of LSPR occurred (about 3 nm) as putative expression on small particle concentration enhancing during irradiation.

During UV-C exposure the LSPR band intensity increased linearly, with linear correlation coefficient $R^2 = 0.93$ (Fig. 6, inset).

In Figs. 7a, b and 8a, b the AgNP optical images recorded in Dark Field mode are presented. Plasmonic emission allowed nanoparticle visualization in Dark Field optical microscopy since the resonant emission reaches a volume of about 2 orders of magnitude higher than the source particles [27]. This way rather rapid imaging and measurement can be accomplished with non-expensive device, non-complicated manipulation, and facile sample preparation [28].

The measurements we have done on the images were conducted with ImageJ with appropriate scaling and calibration and corroborating with electron microscopy investigation results.

The mean diameter of AgNPs before UV-C irradiation (Fig. 7a), estimated from the fitting with the log-normal function, was of 15.1 nm, with Standard Deviation of 5.9 nm (Fig. 7b). Largest particles were found at 35 nm.

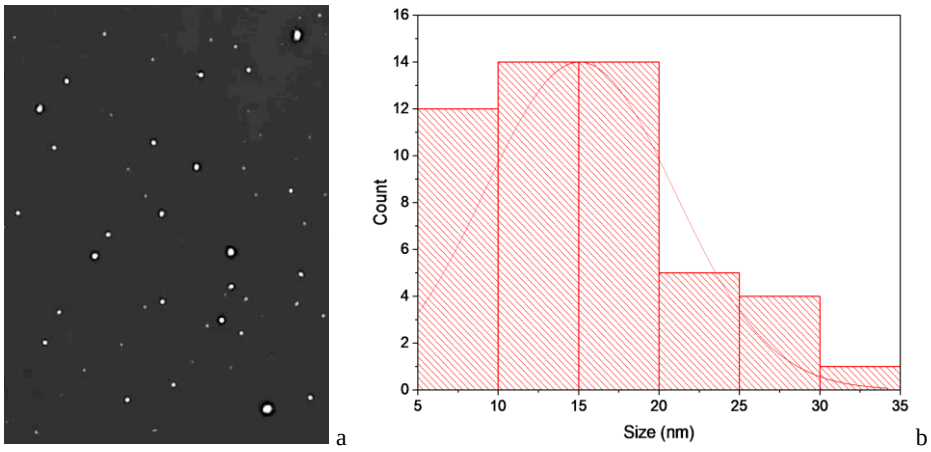

Fig. 7 – a) Dark Field image (40 × objective) for AgNP-TSC before UV-C exposure; b) diameter histogram.

For the irradiated sample, (Fig. 8a, b) the mean diameter, as resulted from the fitting with the log-normal function, was 16.2 nm, with Standard Deviation of 9.6 nm (Fig. 8b). It seems that numerous smaller new particle formation gave histogram asymmetry, with the mean value slightly increased due to the larger particle (or particle aggregates) formation, up to 60 nm, compared to 35 nm in previous case.

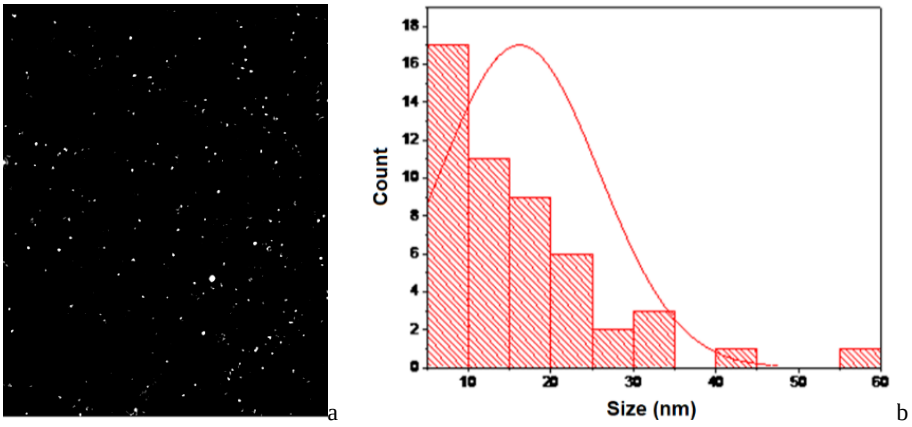

a b

Fig. 8 – a) Dark Field image (40 × objective) for AgNP-TSC after UV-C irradiation; b) diameter histogram.

This suggests that nanoparticle development follows a complex dynamic sustained by the citrate ions attachment to the nanostructures' surface.

We could notice that, under UV-C radiation impact, small particles could form associations of 50–60 nm (Fig. 8b) by losing initial citrate coating and gaining the new citrate larger coating after aggregation.

3.4.2. AgNPs reduced with lemon extract

In Figs. 9-12 the results of UV-C impact on the suspension of AgNP-lemon sample are presented.

The suspension color changed from beige-yellowish to brownish (Fig. 9a, b) denoting the formation of AgNPs stabilized with antioxidants from the lemon extract.

Since it is assumed that the plasmonic spectral band characteristics depend on the optical properties of the surrounding medium [29], the LSPR band maximum depends on the metallic core size but also on the refractive index and the dielectric constant of the molecular shell coating the metallic core [30]. This could underly to the slight differences in the colorations of the two studied suspensions: pale yellow for AgNP-TSC (Fig. 5a) and beige for AgNP-lemon sample (Fig. 9a).

The LSPR characteristic broad spectral band, with the maximum intensity at 430 nm (according to others, like [31]), has the initial intensity of about 0.52 a.u.

The UV-C exposure increased reduction efficacy, thus, the maximum intensity became of about 1.2 a.u. being reached at 425 nm (5 nm blue shift) after 30 minutes

of radiation exposure. Linear dependence of the LSPR band intensity and the UV-C exposure time was evidenced, with linear correlation coefficient $R^2 = 0.84$ (Fig. 10, inset). Lemon extract contains significant concentrations of citric acid and tannic acid, known as highly efficient antioxidants, which have reduced larger amount of silver ions (higher band intensity, 0.52 a.u., compared to AgNP-TSC, with 0.37 a.u.). Hydroxyl ions released through water photolysis has increased LSPR characteristic band (1.2 a.u after UV-C irradiation), about twice compared to AgNP-TSC (with 0.57 a.u.).

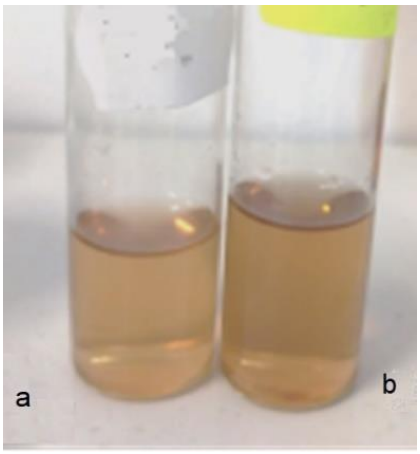

Fig. 9 – AgNP synthesized through the biological method with lemon fruit extract: a) sample before UV-C irradiation; b) sample exposed 30 min to UV-C radiation exposure for 30 min.

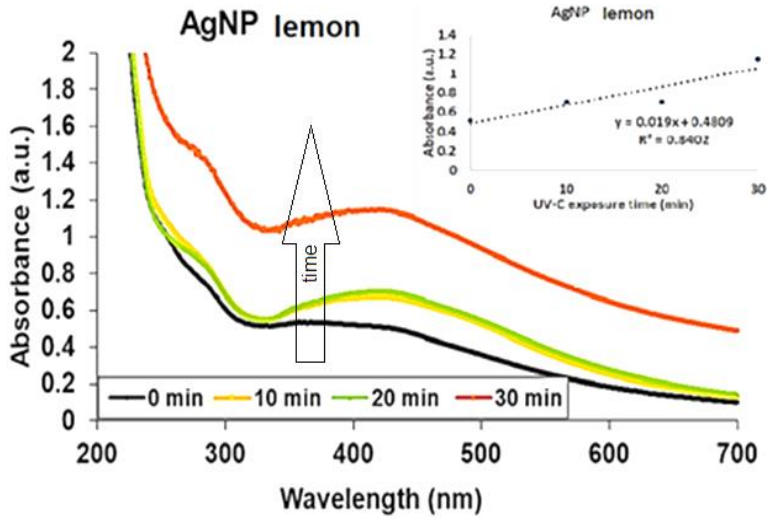

Fig. 10 – The influence of UV-C radiation on the LSPR band of AgNP-lemon.
Image inset-The spectral band intensity increased linearly with UV-C exposure time.

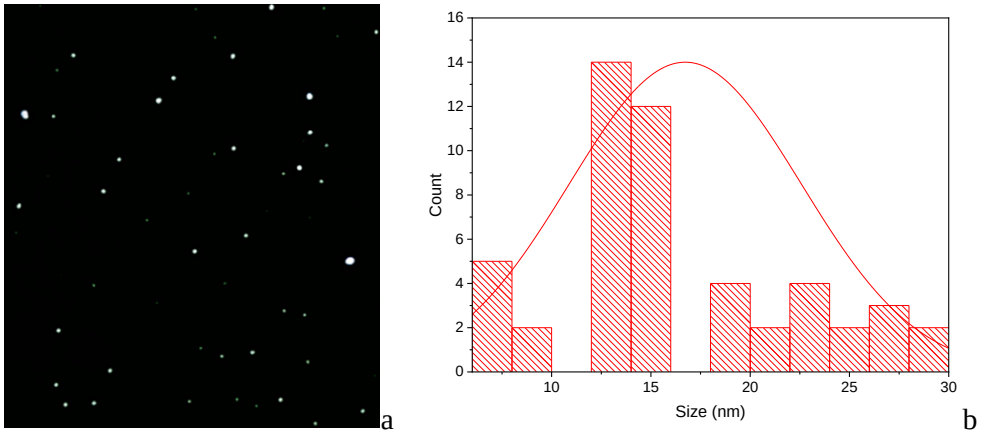

Fig. 11 – a) Dark Field image (40 × objective) for AgNP-lemon before UV-C exposure; b) diameter histogram.

Higher wavelength of LSPR band maximum (at 430 nm before UV-C exposure), compared to the case of AgNP-TSC (418 nm), could be taken as expression of the LSPR position increasing with the particle mean size. And the particle size is larger for AgNP-lemon as shown by SEM analysis (Fig. 1a, b). However, in [32] it was concluded that, in fact no general rule has been found to explain the shifts of the LSPR band, as has been attempted by associating these shifts with changes in size and possibly geometrical shape of the nanoparticles.

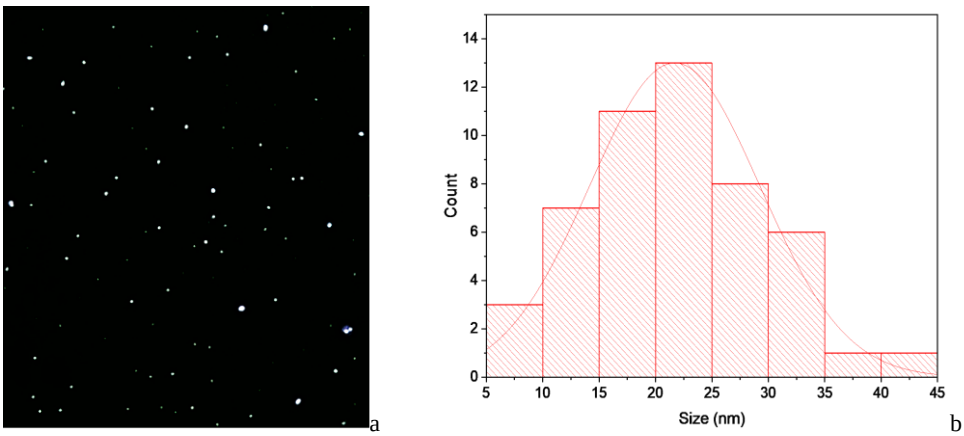

Fig. 12 – a) Dark Field image (40 × objective) for AgNP-lemon after UV-C exposure; b) diameter histogram.

The Dark Field images before AgNP-lemon sample exposure to UV-C radiation in Fig. 11a are exemplified. The mean diameter estimated from the histogram approximation with log-normal function (Fig. 11b) was 16.7 nm, with

Standard Deviation of 5.8 nm. For the AgNP-lemon sample after UV-C irradiation for 30 min, according to Fig. 12a, b, the value of the mean diameter was 21.7 nm, and the Standard Deviation was 7.6 nm with largest particles of no more than 45 nm particles. The mean size enlargement is most probably due also to particle agglomeration during the complex processes that involves new particle formation in the presence of lemon extract organic components. The increased particle size was actually expected to give a LSPR band at larger wavelength than for AgNP-TSC [33] since there is the influence of the surrounding layer formed by larger molecules that influences the properties of the spectral band [34].

We may say that the controlled ultraviolet irradiation appeared as a suitable step in the reaction completion, the synthesized suspensions of the silver nanoparticles remaining stable for two more months in refrigerator conditions. This could represent the main improvement in the proposed synthesis protocol, defined by the specified array of concentrations and volumes of the used reagents. Silver nanoparticles synthesized with fruit extract by two-step photochemical procedure appears as promising eco-friendly production technique aiming various applications in bio-medical fields.

Our results are comparable with those published in literature. In [14] the silver nanoparticles reduced with lemon fruit zest extract were found to have 15.9 nm crystallite size and characteristic spectral band at 535 nm while in [15] the use of lemon fruit peels as well as orange fruit peels has resulted in silver nanoparticles with spectral bands at 430–450 nm and 10–70 nm particles evidenced by electron microscopy. We need to consider that the molecular composition of lemon fruit zest or peels, is not identical to that of lemon fruit extract. In [12] the authors reported AgNPs synthesized with papaya fruits as having 450 nm LSPR position, and average particle size of 15 nm, in [13] the AgNPs synthesized with apple fruit extract were characterized by LSPR band at 441 nm, and 20 nm particle diameter while in [16] the utilization of ananas fruit peels gave AgNPs with maximum absorbance at 463 nm, and crystallite of 11.6 nm. We might say that silver nanoparticles presented in our paper are promising candidates for biologically synthesized AgNPs with optical and spectral features suitable for various utilizations.

4. CONCLUSION

Plasmonic nanoparticles were synthesized with either chemical reducer or biological reducers extracted from lemon fruits by applying two-step procedure that involved UV-C irradiation consecutive to chemical reduction of silver.

The synthesis efficiency increasing with ultraviolet radiation utilization was proved by the enhanced intensity of the characteristic spectral band, with about 50% for AgNP-TSC and with 130% for AgNP-lemon sample. The particle characterization with Dark Field optical microscopy could be a significant benefit in the monitoring

of particle size before and after UV-C exposure. The good results in silver nanoparticle yielding by eco-friendly and low-cost method with fruit extract recommend this approach for large scale particle production. Further, we intend to test AgNP nanotoxicity on young vegetation representative species to highlight the differences between chemical synthesis and biological synthesis ecological threats.

REFERENCES

1. S. Hedberg, M.-E. Skoglund, S. Karlsson, I. O. Wold, Y. Wallinder, and Y. Hedberg, Environ. Sci. Technol. **48**, 7314-7322 (2014).
2. R. Sato-Berrú, R. Redón, A. Vázquez-Olmos, and J. M. Saniger, J. Raman Spectroscopy **40**, 376-380 (2009).
3. B. Calderón-Jiménez, M. E. Johnson, A. R. Montoro Bustos, K. E. Murphy, M. R. Winchester, and J. R. Vega Baudrit, Front. Chem. **5**, 6 (2017).
4. M. K. Hossain, Y. Kitahama, G. G. Huang, X. Han, and Y. Ozaki, Anal. Bioanal. Chem. **394**, 1747-1760 (2009).
5. L. Lu, G. Burkey, I. Halaciuga, and D. V. Goia, J. Colloid. Int. Sci. **392**, 90-95 (2013).
6. X. Dong, X. Ji, J. Jing, M. Li, J. Li, and W. Yang, J. Phys. Chem. C. **114**, 2070-2074 (2010).
7. X. Dong, X. Ji, H. Wu, L. Zhao, J. Li, and W. Yang, J. Phys. Chem. C. **113**, 6573-6573 (2009).
8. K. Ranoszek-Soliwoda, E, Tomaszewska, E. Socha, P. Krzyczmonik, A. Ignaczak, P. Orlowski, M. Krzyzowska, G. Celichowski, and J. Grobelny, J. Nanopart. Res. **19**, 273 (2017).
9. M. Zaarour, M. El Roz, B. Dong, R. Retoux, R. Aad, J. Cardin, C. Dufour, F. Gourbilleau, J.-P. Gilson, and S. Mintova, Langmuir **30**, 6250-6256 (2014).
10. K. J. Hartlieb, A. D. Martin, M. Saunders, and C. L. Raston, New J. Chem. **9**, 1834-1837 (2010).
11. J. Yadav and P. Chauhan, Materials Today: Proceedings **62**, 6177-6181 (2022).
12. D. Jain, H. K. Daima, S, Kachhwaha, and S. L. Kothari, Dig. J. Nanomater. Biostruct. **4**, 557-563 (2009).
13. K. Roy, C. K. Sarkar, and C. K. Ghosh, Dig. J. Nanomater. Biostruct. **9**, 1137-1147 (2014).
14. Y. Khane, K. Benouis, S. Albukhaty, G. M. Sulaiman, M. M. Abomughaid, A. Al Ali *et al.*, Nanomater. **12**, 2013 (2022).
15. M. C. D. Niluxsshun, K. Masilamani, and U. Mathiventhan, Bioinorg. Chem. Appl. **2021**, 6695734 (2021).
16. A. Baran, C. Keskin, M. F. Baran, I. Huseynova, R. Khalilov, A. Eftekhari *et al.*, Bioinorg. Chem. Appl. **2021**, 205814 (2021).
17. J. Kimling, M. Maier, B. Okenve, V. Kotaidis, H. Ballot, and A. Plech, J. Phys. Chem. B. **110**, 15700-15707 (2006).
18. M. Rashid, K. Bhuiyan, and E. Quayum, Dhaka Univ. J. Pharm. Sci. **12,** 29-33 (2013).
19. G. Dhulappanavar, H. Basavaraj, and A. Narasimha, Proc. of Int. Conf. Nanosci. Eng. Technol. (ICONSET 2011) **316**, 258-262 (2011).
20. T. C. Prathna, N. Chandrasekaran, A. M. Raichur, and A. Mukherjee, Colloids Surf. B Biointerfaces **82**, 152-159 (2011).

21. O. Lawal, B. Dussert, C. Howarth, K. Platzer, *et al.*, IUVA news **10**, 14-17 (2008).
22. K. Anandalakshmi, J. Venugobal, and V. J. A. N. Ramasamy, Appl. Nanosci. **6,** 399-408 (2016).
23. B. Gauri, K. Vidya, D. Sharada, and W. Shobha, Res. J. Chem. Environ. **20**, 1-5 (2016).
24. M. Diantoro, R. Fitrianingsih, N. Mufti, and A. Fuad, AIP Conference Proceedings. **1589,** 257-261 (2014).
25. K. Ranoszek-Soliwoda, E. Tomaszewska, E. Socha, P Krzyczmonik, A., Ignaczak, P. Orlowski, and J. Grobelny, J. Nanopart. Res. **19**, 1-15 (2017).
26. J. García-Barrasa, J.M. López-de-Luzuriaga, and M. Monge, Cent. Eur. J. Chem. **9** (1), 19 (2011).
27. A. Weigel, A. Sebesta, P., Kukura, *Dark Field Microspectroscopy with Single Molecule Fluorescence Sensitivity*, ACS Photonics **9**, 848–856 (2014).
28. D. A. Pricop, C. M. Popescu, L. Tartau, and D. Creanga, Appl. Surf. Sci. **621**, 156837 (2023).
29. S. Lee, H. Song, H. Ahn, S. Kim, J. R. Choi, and K. Kim, Sensors **21**(3), 819 (2021).
30. F. Y. Alzoubi, A. A. Ahmad, I. A. Aljarrah, A. B Migdadi, and Q. M. Al-Bataineh, J. Mater. Sci. **34**(32), 2128 (2023).
31. N. J. Alaallah, E. Abd Alkareem, A. Ghaidan, and N. A. Imran, J. Turk. Chem. Soc. A Chem. **10**(1), 205-216 (2023).
32. E. Alzahrani, Anal. Chem. Insights **23**, 1177390116684686 (2017).
33. D. Paramelle, A. Sadovoy, S. Gorelik, P. Free, J. Hobley, and D. G. Fernig, Analyst. **139**, 4855-4861 (2014).
34. H. Chen, X. Kou, Z. Yang, W. Ni, and J. Wang, Langmuir **24**, 5233-5237 (2008).